M. Boiocchi, L. Galfetti, L. Di Landro
Paraffin-Based Solid Fuels for Hybrid Propulsion Filled with Lithium Aluminum Hydride: Thermal, Mechanical, and Ballistic Characterization
International Journal of Energetic Materials and Chemical Propulsion, Vol. 15, N. 6, 2016, p. 501-527
doi:10.1615/IntJEnergeticMaterialsChemProp.2017016259

PARAFFIN-BASED SOLID FUELS FOR HYBRID PROPULSION FILLED WITH LITHIUM ALUMINUM HYDRIDE: THERMAL, MECHANICAL AND BALLISTIC CHARACTERIZATION

Matteo Boiocchi, Luciano Galfetti, Luca Di Landro

Politecnico di Milano, Aerospace Science and Technology Department

I-20156 Milano, Italy

Abstract

A chemical, thermal, mechanical and ballistic investigation of paraffin-based solid fuels filled with Lithium Aluminum Hydride ($LiAlH_4$, LAH) for hybrid propulsion is presented in this paper. Two different formulations containing 5% and 10% of a styrene-based thermoplastic elastomer (Polystyrene-*block*-poly(ethylene-*ran*-butylene)-*block*-polystyrene grafted with maleic anhydride, hereafter named SEBS-MA) were investigated for the strengthening of paraffin waxes. Two LAH mass fractions were considered for each paraffin-based blend (5% and 10%), for a total of four fuel formulations. The paraffin-based blends filled with $LiAlH_4$ were found to be stable when exposed to air. Rheological properties were investigated using a parallel plate rheometer giving evidence of the link between the elastic modulus (G') evolution and the thermal behavior of LAH. Thermal properties were studied using a differential scanning calorimeter (DSC) in order to obtain data about the transitions typical of paraffin waxes (solid/solid and solid/liquid) and also about the thermal decomposition of the added energetic filler. A manufacturing technique for the production of homogeneous blends strengthened with SEBS-MA and filled with LAH is described. Firing tests were performed in a lab-scale hybrid motor using gaseous oxygen; the local and instantaneous regression rate was measured using a fiber optic technique. The behavior of paraffin waxes blended with the selected SEBS-MA thermoplastic elastomer and filled with LAH, is discussed.

Key words: $LiAlH_4$, paraffin wax, thermoplastic elastomer, elastic modulus, differential scanning calorimetry (DSC), fiber-optic

NOMENCLATURE

CB	:	Carbon Black
DSC	:	Differential Scanning Calorimetry
FO	:	fiber optics
G	:	mass flux, *kg/(m²s)*
G'	:	elastic modulus, *Pa*
G_{OX}	:	gaseous oxygen
H	:	specific enthalpy, *J/g*
LAH	:	Lithium Aluminum Hydride ($LiAlH_4$)
O/F	:	oxidizer to fuel ratio
r_f	:	fuel regression rate, *mm/s*
SEBS-MA	:	Styrene-Ethylene-Butylene-Styrene copolymer, grafted with Maleic Anhydride
T	:	temperature, *°C*
TOT	:	thickness over time

Greek Symbols

Δ	:	difference
M	:	viscosity, *Pa*s*
P	:	density, g/cm^3

Subscripts

Dec	:	decomposition
Liquid	:	liquid
Lim	:	limit
M	:	melting
Fin	:	final

1. INTRODUCTION

Paraffin waxes represent an important class of solid fuels for hybrid propulsion because of the remarkable increase in regression rate which is possible to obtain (Karabeyoglu et al., 2001; Karabeyoglu et al., 2004) compared with traditional fuels (Chiaverini et al., 2000; Altman, 2003; Oiknine, 2006; Davydenko et al., 2007). The melting of these fuels forms a thin, hydrodynamically unstable liquid layer on the surface and the entrainment of droplets from the liquid–gas interface increases the rate of fuel mass transfer (Karabeyoglu et al., 2002). Due to the well-known unsuitable mechanical properties (Maruyama et al., 2011) typical of pure paraffin waxes, an increase of elasticity and toughness is mandatory in order to use paraffin wax as solid fuel for hybrid rockets. Two different formulations containing 5% and 10% of a styrene-based thermoplastic elastomer (Polystyrene-*block*-poly(ethylene-*ran*-butylene)-*block*-polystyrene grafted with maleic anhydride, named SEBS-MA) were investigated for the strengthening of paraffin waxes (Prasman et al. 1997; Kim et al., 2006; Zhang et al., 2012). Several kinds of energetic fillers for hybrid propulsion have been widely studied; among them metal hydrides are probably the most interesting from several points of view. The combustion of metals is highly exothermic and, moreover, the presence of hydrogen leads to various energetic and propulsive benefits (Block and Gray, 1964; McLain and Honea, 1969; Humble, 2000) such as the enhancement of the energetic content of the fuel, the increase of the specific impulse and regression rate (Osmon, 1966; Shark 2013). The most important parameters suitable to define a good metal hydride to be used in space propulsion applications are the density value and the hydrogen content. Both must be as high as possible. The best solution is represented by AlH_3, because of its high specific impulse and its high density value. Unfortunately, Aluminium hydride is not a commercial product. For this reason metal hydride powders, commercially available and cheaper should be considered, with a lower, but acceptable, specific impulse value. Among them a good trade-off between physical and economical characteristics is given by Lithium Aluminum hydride ($LiAlH_4$), which was studied as main double metal hydride in a number of fuel formulations for hybrid propulsion applications. The sensitivity to moisture, which is the most serious drawback of lithium aluminium hydride (LAH), was studied exploiting the hydrophobic behavior typical of the paraffin wax. The paraffin-based blends filled with LAH were found to be stable when exposed to air. Two LAH mass fractions (5% and 10%) were investigated for each paraffin-based blend, for a total of four fuel formulations. A deep knowledge of the thermal, rheological and mechanical behavior of these blends is important in order to reach a good trade-off between mechanical and ballistic properties. A paraffin wax, investigated and analyzed in a previous study by mass spectrometer gas-chromatographic

technique (GC-MS) (Boiocchi et al., 2016), was selected. For this wax information was obtained about the de-oiling grade, which affects both the rheological and mechanical properties.

2. EXPERIMENTAL DETAILS

2.1. Investigated materials

Paraffin waxes are a mixture of hydrocarbons, mainly normal alkanes. Carbon numbers span in the range approximately between 18 and 45. Paraffins are rather weak and brittle and for this reason they are ill-suited for applications requiring appropriate mechanical properties, such as the solid fuel of a hybrid rocket engine. Research efforts are devoted to develop high performance materials with a greater stiffness and a greater elongation at break.
The selected paraffin was a commercial paraffin supplied by an Italian Company, hereafter named GW, with a DSC melting point of 54.9 °C. Paraffin was mixed with SEBS, which is a styrene-ethylene-butylene-styrene block copolymer, grafted with maleic anhydride (SEBS-MA), supplied by Sigma Aldrich. Different compositions were manufactured and characterized, according to the list and the nomenclature of Table 1. The mixing between SEBS and wax was obtained firstly by melting a 50/50% mixture under stirring at 120 °C; when the mixture became homogeneous the last part of paraffin was added reducing the temperature at 90 °C. The last ingredient to be added was carbon black. A good temperature control during all these operations is strictly needed in order to prevent the thermal degradation of SEBS-MA and, at the same time, to avoid the partial evaporation of the lighter carbon fractions contained in the paraffin wax. For paraffin-based mixtures, it is generally true that the higher the temperature of the melt is, the stronger the shrinkage effect of the mixture into the mold during the cooling.

Table 1: Composition and theoretical density of pure paraffinic materials and SEBS-based blends investigated in this study.

Fuel	Composition	Theoretical Density [g/cm^3]
GW	Macro-crystalline Paraffin Wax	0.870
SEBS	Styrene 30% Maleic anhydride 2%	0.910
S05G	SEBS 5% GW 94% CB 1%	0.883
S05G-L5	95% (SEBS 5% GW 94% CB 1%) + 5% LAH	0.885
S05G-L10	90% (SEBS 5% GW 94% CB 1%) + 10% LAH	0.886
S10G	SEBS 10% GW 89% CB 1%	0.885
S10G-L5	95% (SEBS 10% GW 89% CB 1%) + 5% LAH	0.887
S10G-L10	90% (SEBS 10% GW 89% CB 1%) + 10% LAH	0.888

2.2. Thermal characterization

The Differential Scanning Calorimetry (DSC) measurements of the materials studied in the present work were performed using a TA Instruments model 2010 CE thermal analyzer system. The calibration was performed with an Indium standard; all the experiments were performed by using nitrogen gas (33 ml/min) as heating/cooling gas and tested at 10 K/min as temperature ramp. All the sample tested were weighed by a Mettler Toledo electronic balance (0.1 mg accuracy) and the sample mass ranged between 2.80 and 3.05 mg.

2.3. Viscoelastic characterization

In order to obtain the viscoelastic behaviour of the investigated formulations a rotational rheometer was used. All the experiments were carried out by a *Rheometrics Dynamic Analyzer RDA II*. This setup works in an oven in which an air flux allows to establish a temperature-controlled regime during the test.

Viscoelastic characterization: dynamic viscosity

A Couette apparatus for viscosity measurements on melted materials was used. This apparatus works in an oven in which an air flux allows to establish a temperature-controlled regime during the test. The outer cylinder rotates, while torque is sensed on the inner non-rotating cylinder. Particular attention must be paid during the pouring of the melted material in order to prevent bubble gas formation. A test using this kind of rheological apparatus is usually performed in controlled-rate mode with the shear rate ranging logarithmically between 5 s^{-1} and 1260 s^{-1}. The test temperature values ranged between 85 and 165 °C.

Viscoelastic characterization: rheology

All the experiments were carried out by a *Rheometrics Dynamic Analyzer RDA II* using a parallel plate apparatus to study the elastic modulus (G'). This apparatus works in an oven in which an air flux allows to establish a temperature-controlled regime during the test. The lower plate rotates, while torque is sensed on the inner non-rotating plate. Parallel-plate tests were performed considering small amplitude sinusoidal oscillatory testing as function of test frequency. The test temperature values ranged between 19 °C and the melting point, with 3 °C of spacing between each test. The usual range of frequency values in which all the tests were performed was from 0.5 to 50 Hz. All rheological tests were performed using a thin disk (25 mm diameter, 1 mm thickness) of the material under investigation, placing it between the plates of the rheometer and increasing the temperature so as to obtain a partial melting of the material in direct contact with the metal. The rheological test usually started as the temperature of the sample was stabilized at the ambient value. This operation was necessary to allow a good physical contact between the plates of the setup and the disk of the paraffin-based material under testing.

2.4. Ballistic properties

The firing tests were carried out using a lab-scale hybrid test facility designed and developed at SPLab. A schematic overview of the experimental test bench used in the present work is shown in Figure 1a. A schematic description of the fiber optic experimental facility used to obtain a punctual, quasi-continous measure of the regression rate of a fuel during a firing test is shown in Figure 1b.
Fiber-optic sensors represent one of the most innovative techniques (Benterou and Udd, 2007; Udd and Benterou, 2010) to measure very high speed events such as velocity of detonation in explosives. Commercial fiber optic in combination with relatively inexpensive commercial electronic instruments can be used to measure the combustion rate of hybrid fuels. An experimental set-up was implemented at SPLab and some preliminary firing tests were conducted with a complete non-intrusive apparatus based on fiber optic ribbon. The commercial ribbon usually used during the experimental investigation was a 12-fiber ribbon with a regular spacing of 250 μm, connectorized at one head end to match with the analyzer. The free head end of each optical fiber of the ribbon was opportunely sealed with a ceramic material and leaned to the fuel

inside the combustion chamber. An electronic analyzer consisting in an array of 8 photodiodes (named: Light Intensity Analyzer 8 channels LIA08) was used to turn a luminous signal into an electrical signal. Finally, a plot reporting the trend of the light intensity of eight luminous signals versus time was obtained and used to calculate the regression rate value. Each fiber in this experimental configuration could be treated as a luminous switch: on/off. When the combustion surface is far from the first fiber each one is in the dark, so all the electrical signals from the photodiodes array are negligible. As the luminous region of the flame approaches to the array of fiber optics, more than one fiber is able to collect photons to the corresponding photodiodes thanks to the not perfect opacity of the fuel. Compared with the intensity of the flame region the light diffused below the combustion surface is negligible. Another interesting point is linked to the intrinsic characteristic of the fiber optic: to have an optimal propagation of the light into the fiber, the angle between the light source and the fiber core axis has to be less than a critical angle. In another arrangement developed at SPLab the fiber optics array is cut with an angle in such a way that the distance between the longest and the shortest fibers is approximately 5 mm. The array is put into the core hitch in the combustion chamber so that the longest fiber is in contact with the mandrel of the mold. Blocking the relative position of the array in the core hitch, it is possible to cast the fuel. It is possible to obtain the required information of regression rate by knowing the correct spacing of each fiber and the difference in time between each luminous signal.

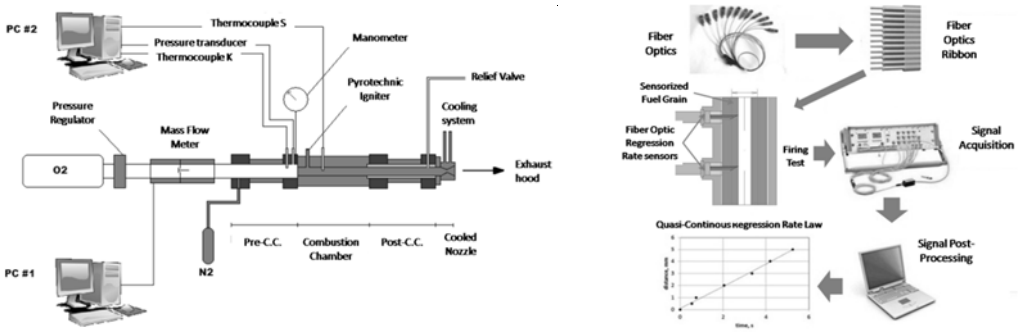

Figure 1. (1-a, left) Schematic layout of the experimental test bench ; (1-b, right) Schematic of the fiber optics facility.

3. RESULTS

3.1. Thermal characterization

Figure 2 shows the DSC scan of the GW paraffin and its blends used throughout this study. The scan shows the heating cycle: the transition temperature starts at about 28 °C, with a peak at 36 °C, corresponding to the pre-melting solid-solid transition. The higher transition temperature, which is the same for both the selected formulations (peak at 55°C), is the melting transition temperature. The high-temperature endothermic peaks, occurring between 190 °C and 300 °C, are due to the gasification/decomposition processes.

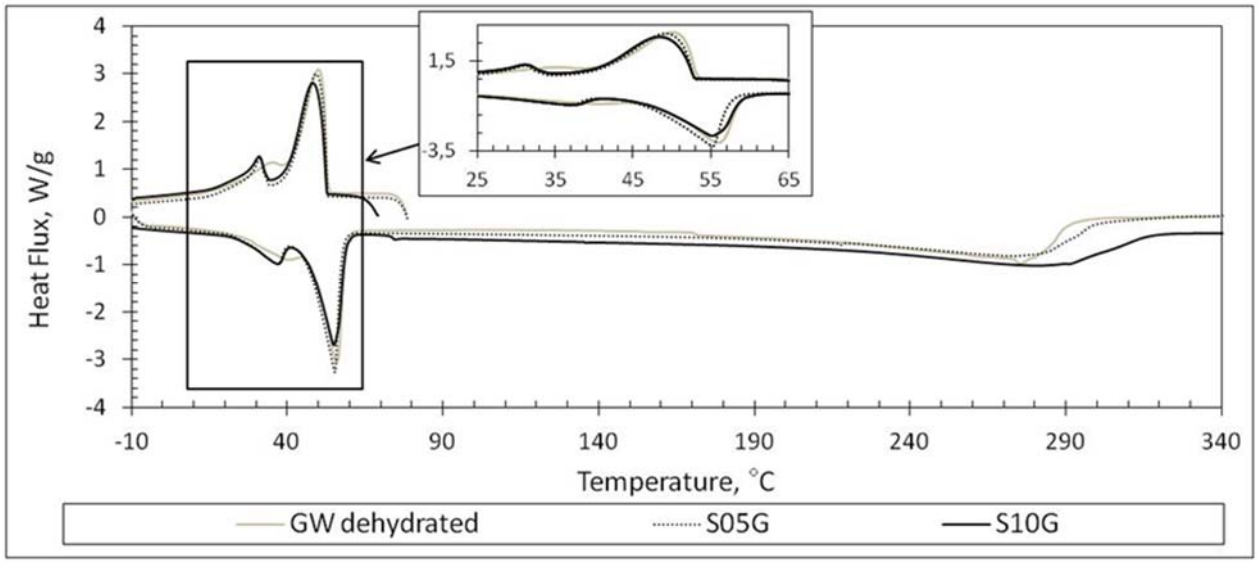

Figure 2. DSC scan of dehydrated GW and its blends containing 5% and 10% of SEBS-MA.

A typical macro-paraffin endothermic thermograph is usually composed by two well-defined peaks: the first, corresponding to the solid-solid transition, and the second corresponding to the solid-liquid transition. Considering the exothermic part of the DSC trace, specular to the endothermic trace, two well-defined peaks can be detected. The main exothermic peak is linked to a liquid-solid transition and it is followed by a peak showing a solid-solid transition. Considering Figure 2 and Table 2, a temperature shift of about 5-6 °C can be seen between each endothermic peak and its homologous exothermic peak. This behaviour, named supercooling (Royon and Guiffant, 2001) is given, by definition, by the difference between the temperature of solid/liquid transition and the temperature of liquid/solid transition. According to the literature (Chazhengina et al., 2003; Alcazar-Vara and Buenrostro-Gonzalez, 2013) on heating, some macro-paraffin waxes show a transition from an ordered monoclinic crystal structure to a disordered pseudo-hexagonal crystal re-arrangement. Increasing the temperature of the DSC oven over 200 °C, the thermal behavior of GW is shown in Figure 2; an endothermic peak between 190 °C and 300 °C attributed to the gasification/decomposition of the samples can be observed. Considering the blends of GW with SEBS-MA polymer shown in Figure 2, the absence of the thermal shift of the main endothermic peak is noticed. A similar behaviour was observed (Seno and Selvin, 2006) by performing blends with SEBS-MA and Polyamide12. The measured melting point of GW was 56.0 °C; when the thermoplastic polymer was added (5% and 10% mass fraction), the main peak temperature was between 55.3 and 55.2 °C. This trend is due to the amorphous nature of the polymer or to its very low grade of crystallinity. The DSC trace does not show any relevant endothermic or exothermic peak, as illustrated in Figure 2. In a mixture between a paraffinic material and an amorphous material only the waxy material is detectable by DSC, which gives a signal directly proportional to the paraffin mass fraction. An inverse proportionality between melting enthalpy (ΔH_m) and polymer mass fraction (from 5% to 10%), reported in Tab. 2, was observed. In order to understand the thermal behaviour of SEBS-MA, a DSC analysis was performed. SEBS-MA was confirmed to be amorphous; only a negligible peak in the temperature range 30-50 °C was evidenced, which can be attributed to trace of crystallinity of rubber (Ethylene Butylene, EB) blocks (Mingjie Zheng and Weimin, 2006). Another influence of the polymer content in SEBS-based mixtures detected in DSC thermographs was linked with the temperature of the solid-solid transition peak both in heating and cooling.

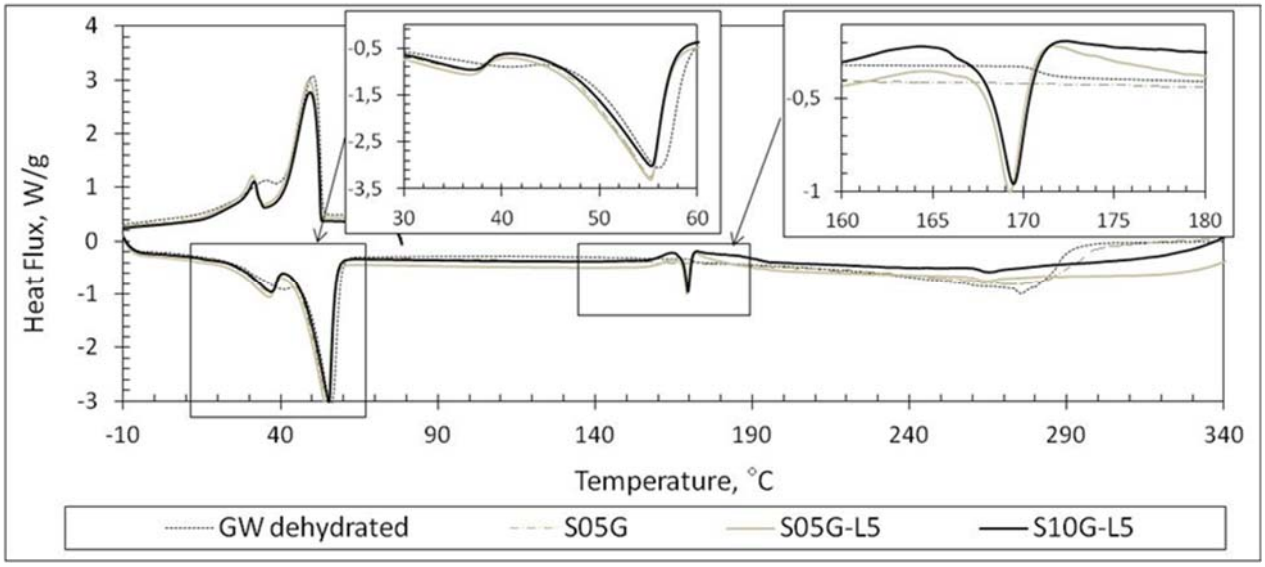

Figure 3. DSC thermographs of S05G-based formulations containing 5% and 10% of LAH.

As shown in Figure 3 as the LAH powder is added to the mixtures, the typical decomposition double peak can be observed in the temperature range between 150 and 190 °C. The content of LAH does not affect the behaviour of the melting temperature, as shown in the magnification at top of the plot in Figure 3. Looking at the magnification in the right high corner of Figure 3, as the LAH content increases, the enthalpy of decomposition also increases (from 24.8 to 46.5 J/g considering S05G-based blends, from 18.5 to 48.3 J/g for S10G-based formulations).
When the GW content in the considered blends decreases, ΔH_{dec} also decreases for all the formulations, except for those containing a mass fraction of 10%, which show an increase. The decrease can be explained considering that the DSC trace is affected by the GW crystallinity. SEBS is amorphous and LAH at that temperature should be decomposed. A less pronounced peak is detected for the formulations with a lower GW content. The increase is linked to the amount of the filler; despite several steps of the filler thermal degradation being below the temperature of 250 °C, the filler is still able to release energy. The effect is larger when the amount is greater.

Table 2: Parameters obtained from DSC measurements for paraffinic waxes
('T' temperature, 'ΔH' specific enthalpy, 'm' melting, 'dec' decomposition).

Material	Mass [mg]	$T_{m,p}$ 1 [°C]	$T_{m,p}$ 2 [°C]	ΔH_m [J/g]	T_{dec} 1 [°C]	T_{dec} 2 [°C]	T_{dec} 2 [°C]	ΔH_{dec} [J/g]	T_{dec} 1 [°C]	ΔH_{dec} [J/g]
LAH	2.82	-	-	-	162.0	167.3	189.0	754.8	257.2	211.8
GW	2.84	36.8	56.0	206.2	-	-	-	-	275.4	185.4
S05G	2.90	36.7	55.3	198.3	-	-	-	-	273.2	154.9
S05G-L5	2.90	36.4	55.1	193.2	164.4	169.2	171.6	24.8	264.7	24.9
S05G-L10	2.91	36.7	55.2	181.1	166.6	169.2	171.1	46.5	263.1	84.6
S10G	2.96	37.4	55.2	188.6	-	-	-	-	278.2	92.1

S10G-L5	2.81	37.0	55.2	179.2	164.4	169.4	172.3	18.5	265.1	45.3
S10G-L10	2.86	36.9	55.2	171.3	164.2	169.5	172.3	48.3	264.1	94.7

A comparison between two S05G-based fuels filled with LAH and a pure sample of metal hydride, is shown in Figure 4. A remarkable energy release (754.8 J/g) of the pure LAH powder can be observed in Table 2. Looking at the decomposition magnification in the range between 155 and 195 °C the decomposition peaks of pure LAH and of the two investigated blends approximately occur at the same temperature. Looking at Table 2, it is possible to check that when the LAH amount increases the two peaks do not shift significantly (164 °C for the first exothermic peak, 171 °C for the endothermic peak, and 171-172 °C for the second exothermic peak).

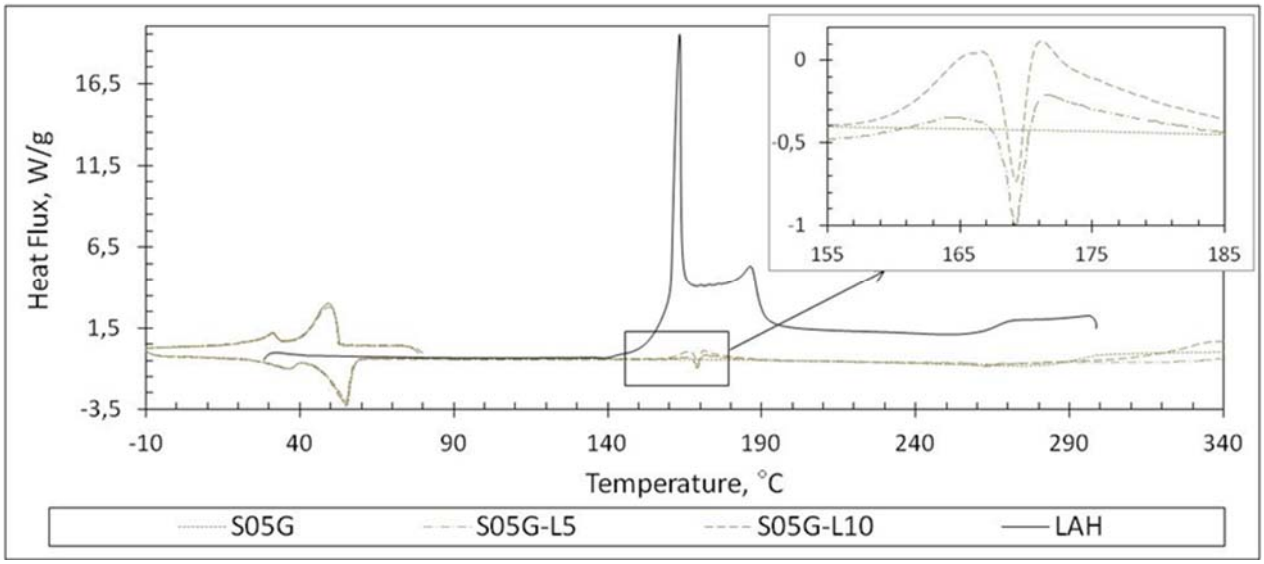

Figure 4. DSC trend of two S05G-based blends filled with 5% and 10% of LAH compared with a pure sample of Lithium Aluminium hydride.

3.2. Viscoelastic characterization: dynamic viscosity

Figures 5, 6 and 7 show the viscosity trend (Couette tests) of the formulations S10G-based between 80 and 120 °C. When temperature increases, viscosity decreases for all the tested formulations.As aspected, increasing the LAH content, the viscosity increases for all the formulations S10G-based. An opposite behaviour was observed taking into account the formulations S05G-based in which the viscosity values measured at 70°C decreases from 0.5 to 0.183 Pa*s despite the increasing of the LAH content. This behavior could be ascribed to a partial sedimentation of the LAH powder due to the low content of SEBS. Another reason could be also linked to the whole time at which the mixture is maintained at high temperature. A similar observation was taken when formulations SEBS-free were performed to prepare samples for the ballistic characterization of a previous work (Boiocchi, 2012). In order to prevent the sedimentation of the powder it was necessary to mix the LAH to the paraffin wax only few degrees above the melting point and then, by pouring into the mould, obtaining a fast freeze of

the wax. This behavior was observed also in waxy formulations containing 10% or more of SEBS, but at temperature values higher than 120°C. For this reason, as it can be seen in Table 3, the viscosity values at 140°C and !60°C were not taken. Considering again the behavior observed in the formulations S05G-L5 and S05G-L10, an amount of only 5% of SEBS is not enough to increase the viscosity at 70°C or more, to prevent the sedimentation of LAH powder. Table 3 shows that for all formulations added with the filler, the temperature range does not exceed 120 °C as, at this stage, the measurement is difficult because of hydride decomposition, forming gaseous H_2 in the Couette rheometer air space. Choosing from Table 3 the viscosity values of S10G-based formulations measured at a rotation speed of 400 s^{-1}, and plotting these values with the homologous DSC curves, this phenomenon can be detected from a different point of view. Figure 8 shows that at 120 °C, far from the LAH decomposition temperature (between 155 e 190 °C), the hydride de-hydrogenation becomes significant. Figure 13 shows the surface of a fuel S10G-L5 based, and the condition of the material below the regression surface. LAH de-hydrogenation, above 172 °C causes a reinflating of the material due to the gaseous hydrogen. This phenomenon is responsible also for the different regression rate value obtained using fiber optics and weighing the sample before and after a firing test.

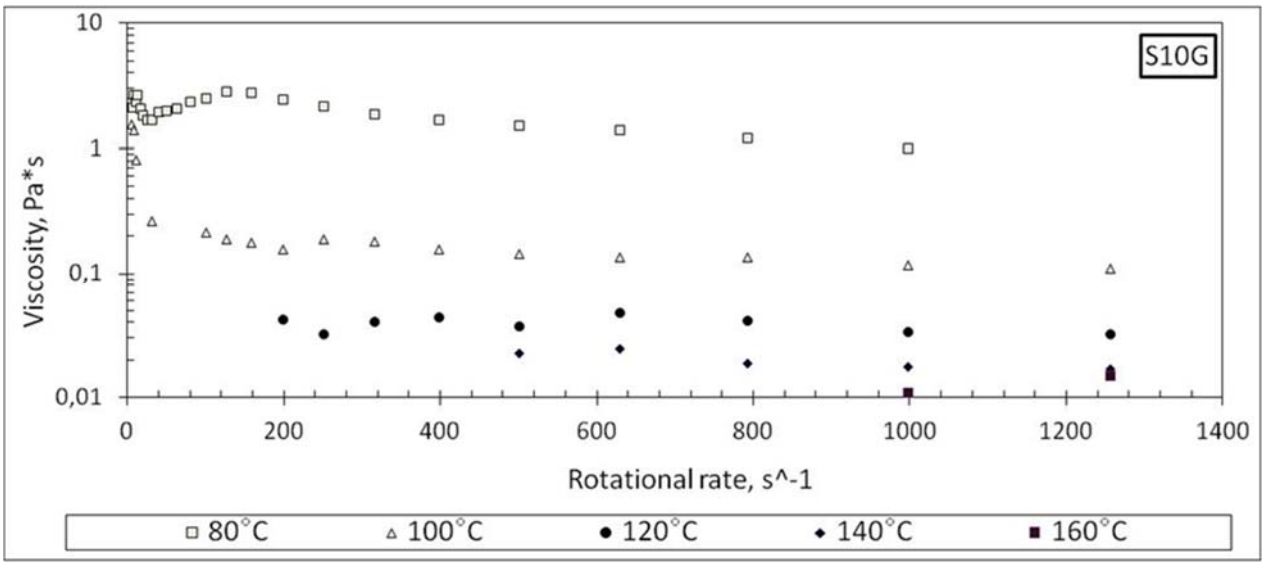

Figure 5. Trend of viscosity for S10G at different temperature values.

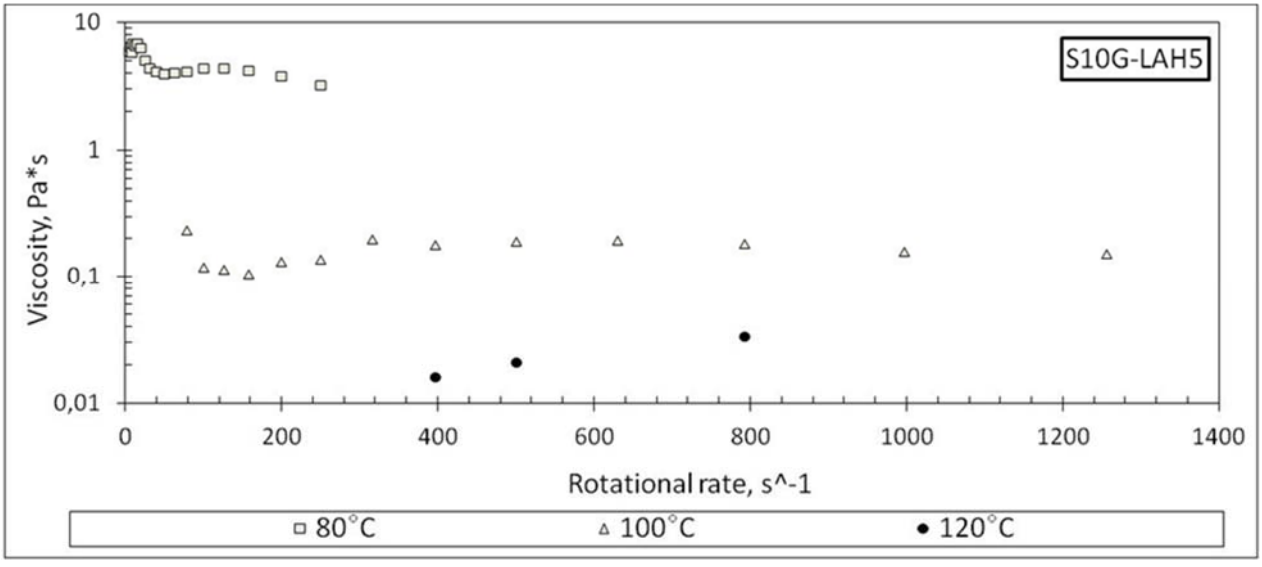

Figure 6. Trend of viscosity for S10G filled with LAH 5% at different temperature values.

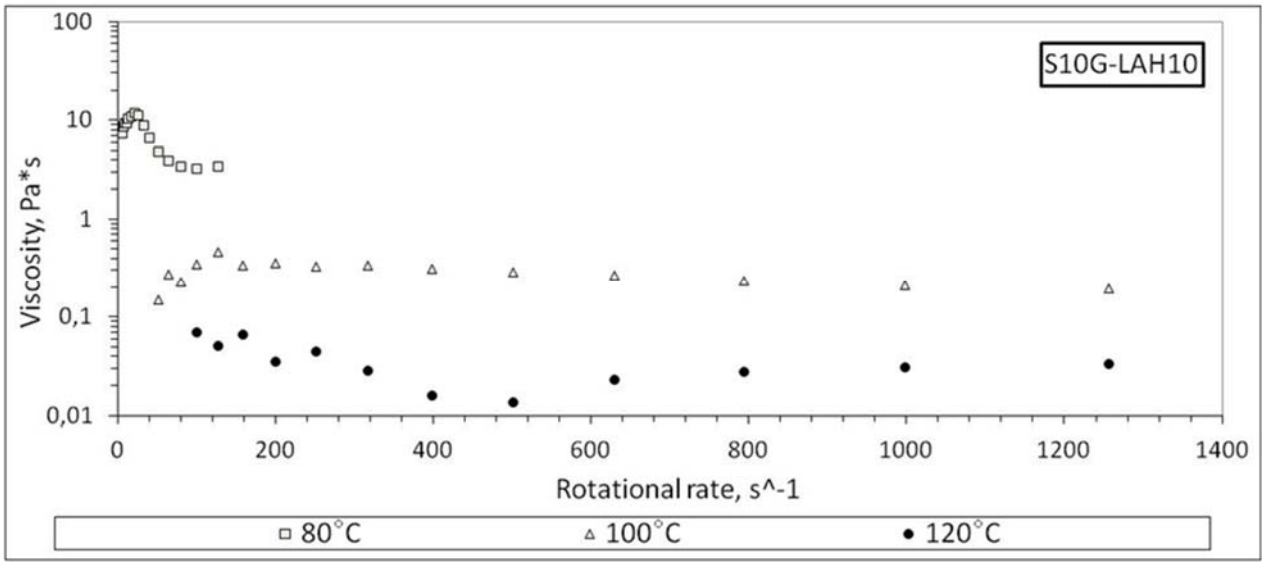

Figure 7. Trend of viscosity for S10G filled with LAH 10% at different temperature values.

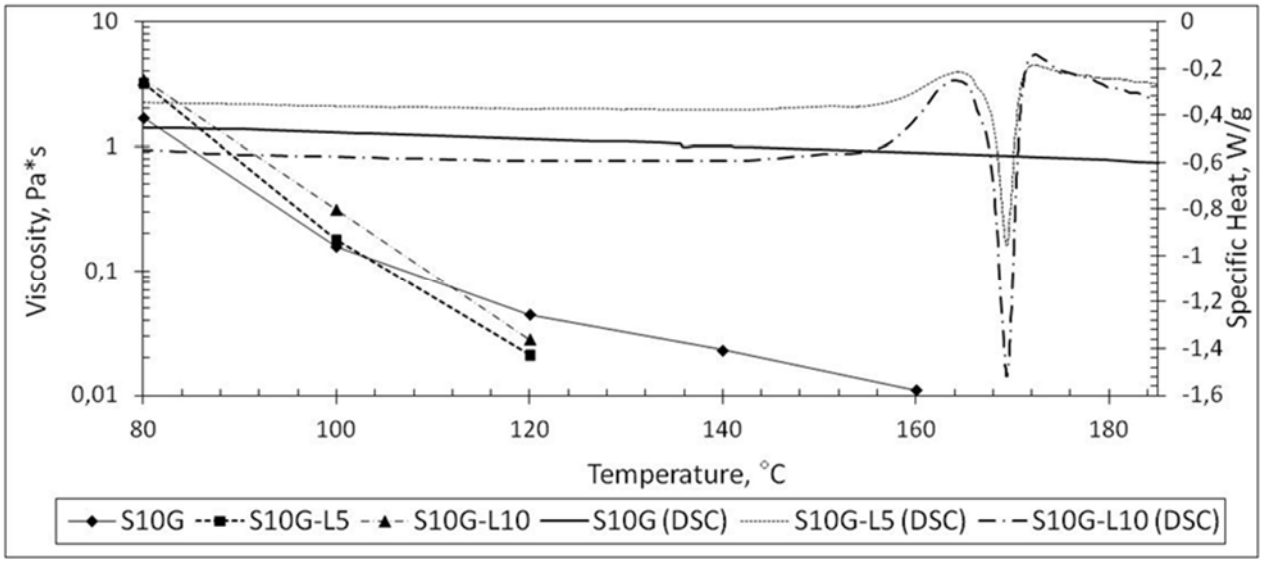

Figure 8. Viscosity trend for S10G-based mixtures compared with the respective DSC thermographs between 80°C and 160°C.

Table 3: Viscosity values obtained with Couette rheometer tests at 400 s^{-1}.

Mixture	**Viscosity [Pa*s]**					
Temperature	**70**	**80**	**100**	**120**	**140**	**160**
S05G	0.50	0.123	0.046	-	-	-
S05G-L5	0.244	0.044	0.032	-	-	-
S05G-L10	0.183	0.041	0.037	-	-	-
S10G	-	1.694	0.157	0.044	0.023	0.011
S10G-L5	-	3.228	0.18	0.021	-	-

S10G-L10	-	3.437	0.313	0.028	-	-

3.3. Viscoelastic characterization: rheology

Figures 9 shows the trend of the elastic modulus (G') for S05G-based mixtures compared with the respective DSC thermographs in the range between 15 °C and 60 °C. The shift occurring between the endothermic peak pointed out by DSC test and the beginning of G' sharp decrease is due to the different mass of the samples (2 mg vs. 2 g). Different masses are characterized by different thermal inertia. A preliminary investigation on the rheological behaviour of the selected materials was performed by determining the elastic modulus response by variation of the percentage strain value. A value of percentage strain of 1% was selected as a good trade-off between the needed stress/strain linearity and the sensitivity of the test bench. The overlapping with DSC traces allows an interpretation of the softening behavior of a typical macro-crystalline paraffin. The LAH contribution is very weak. Considering the maximum temperature at which the sample is able to deliver a torque, the formulation containing 10% of LAH exceeds 49 °C, typical of the pure blend, and the formulation containing 5% of the filler reaches 52 °C.

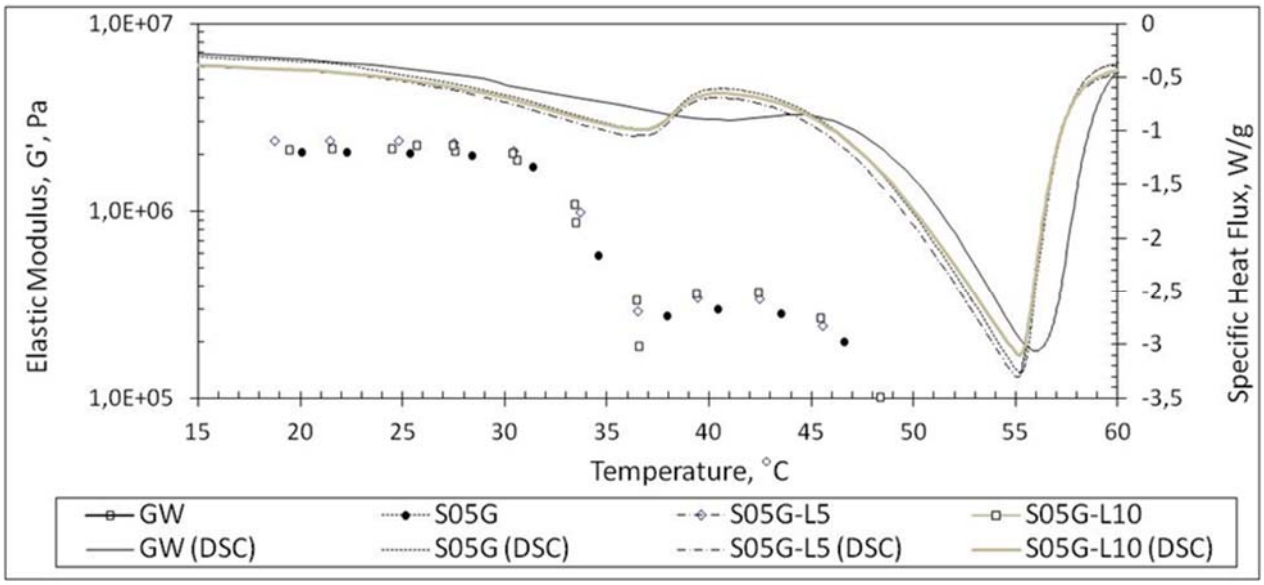

Figure 9. Trend of the elastic modulus (G') for S05G-based mixtures compared with the respective DSC thermographs between 20°C and 60°C.

An example of shift between heating and mechanical properties, due to the LAH presence, is shown in Figure 10.

If a rheological test is performed on a material sample previously submitted to a Couette test at 140 °C, a change in the material behavior can be detected. The treated material remains thermoplastic but develops a strength to temperature greater than the fresh material (T_{max} = 65 °C vs. 55 °C). The magnification in Figure 10 shows that the change of the material mechanical properties is linked to a decreasing of the area of the LAH decomposition peak (from 48.3 a 0.2 J/g). This means that the test performed at high temperature with the Couette rheometer causes a strong decomposition of the hydride, which is no more detected by DSC, and at the same time causes an increase of the melting temperature of the compound partially degradated (T_{liq} > 65 °C) when compared to the fresh (T_{liq} > 49 °C).

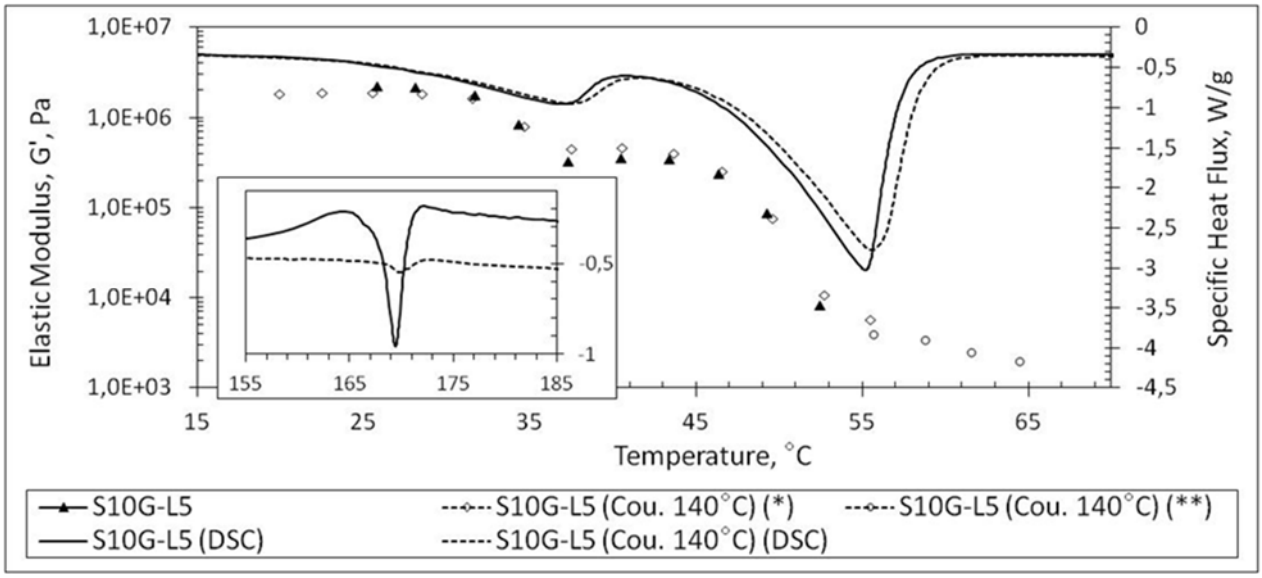

Figure 10. Trend of the elastic modulus (G') for S05G-L5 tested fresh and after a Couette experiment performed at 140°C. The same sample was tested imposing 1% strain (*) and then 4% strain (**).

Table 4: Parameters obtained from DSC measurements for paraffinic waxes.
('T' temperature, 'ΔH' specific enthalpy, 'm' melting, 'dec' decomposition, '*' after Couette test at 140°C).

Material	Mass [mg]	$T_{m,p}$ 1 [°C]	$T_{m,p}$ 2 [°C]	ΔH_m [J/g]	T_{dec} 1 [°C]	T_{dec} 2 [°C]	T_{dec} 2 [°C]	ΔH_{dec} [J/g]	T_{dec} 1 [°C]	ΔH_m [J/g]
S10G	2.96	37.4	55.2	188.6	-	-	-	-	278.2	92.1
S10G-L10	2.86	36.9	55.2	171.3	164.2	169.5	172.3	48.3	264.1	94.7
S10G-L10*	3.02	37.4	55.6	173.8	-	169.8	172.8	0.2	264.3	40.3

The shift occurring between the endothermic peak pointed out by DSC test and the beginning of G' sharp decrease was probably linked to the different mass of the samples (2 mg vs. 2 g), involving a different thermal inertia. Two critical temperatures define the G' trace into three main areas. The first one lasts until the solid/solid transition occurs: the G' values are almost constant and frequency independent. The second can be identified between the solid/solid and the solid/liquid transition of the paraffin: the blend transmits a torque to the rheometer sensor, but, because of the swelling process, an intense dependence of G' values on percentage strain was observed. The last one can be associated to the temperature range between the solid/liquid transition and a limit temperature (T_{lim}) just before the complete melting of the mixture. DSC tests point out that the peak where GW melting occurs is at 54 °C. The decrease of the elastic modulus of pure SEBS-MA starts at 80 °C. Investigations to study structural morphologies (Reynders et al., 1995; Laurer et al., 1996; Kleppinger et al. 1998; Kleppinger et al. 1999; Wilkinson et al. 1999; Asthana and Kennedy, 2002; Litmanovich et al., 2002) and viscoelastic and thermal properties of styrene-based thermoplastic elastomers and their blends with different polymers and fillers (Laurer et al., 1998a; Laurer et al. 1998b; Dezhen et al., 2004; Wang et al., 2008; Pracella et al., 2010) were performed. The results show that gels rheological and mechanical properties are affected by block copolymer concentration, molar mass, end-block ratio and chemical compatibility with the filler. Mechanical properties when SEBS-MA is mixed

with polymers (e.g. Nylon 6 or Polyamide 6) were investigated in order to open the maleic anhydride rings creating stable chemical bonds (or crosslinks). In such cases SEBS-MA is usually used as impact modifier or compatibilizer (Horiuchi et al. 1997; Wilkinson et al. 2004; Huang et al. 2006; Chow et al. 2012) improving both impact and toughness characteristics. SEBS-MA was chosen after a preliminary experimental investigation about the use of thermoplastic polymers as strengthening materials for paraffin-based formulations. SEBS-MA were studied both from a ballistic and rheological point of view indicating the maleated formulation as the best choice. Considering the same experimental conditions (storing temperature, polymer mass fraction and polystyrene mass fraction), not-maleated polymer-based blends have shown low regression rate and scarce toughness.
DSC tests point out that the peak where GW melting occurs is at 54 °C. Thermographs of formulations containing 5% and 10% mass fractions of SEBS-MA seem to be characterized by the same melting temperature of pure GW.

3.4. Ballistic results

A typical result showing fiber optics (FO) signals and pressure is reported in Figure 11-a. Figure 11-b shows the usual look of the combustion surface containing a unfilled formulation after a firing test. It is clearly visible the presence of the fiber optic sensor head-end coming out from the combustion surface roughly of a 1 mm.

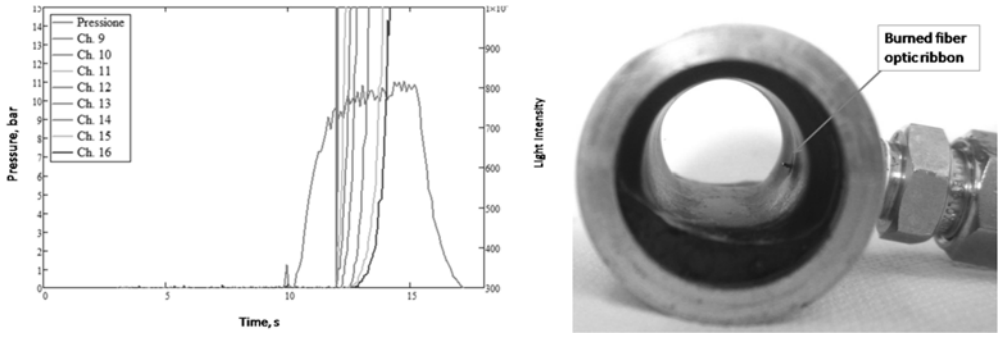

Figure 11. (11-a, left) Typical plot reporting the evolution of pressure during combustion and luminous signals collected by a 8 channels fiber optic sensor; (11-b, right) Fuel surface after 5 sec of combustion with a fiber optic ribbon head-end sensor.

The results obtained during the ballistic characterization (mass flow setted between 3.6 g/s to 5.5 g/s of pure gaseous oxygen) are listed in Table 5. One can see the regression rate values obtained using two different measuring techniques, the oxygen mass flux (G_{ox}), the measured O/F ratio the equivalence ratio and the pressure. The values of the adiabatic flame temperature and the maximum specific impulse, both calculated using the NASA CEA2 code, were also reported. The measured value of the O/F ratio was obtained dividing the imposed oxygen mass flow by the measured fuel mass flow. The last parameter was calculated dividing the fuel mass consumption by the time of combustion.
Taking into account the fuels S05G-L5 and S10G-L10, it can be seen that increasing the value of G_{ox} from 72.4 Kg/m^{2}s to 90.5 Kg/m^{2}s, a decrease of the value of measured O/F was observed for both the formulations.

An explanation could be linked with the burned fuel mass which, for the both formulations, has grown more than that of the other formulations. Due to the fact, then, that the time of combustion was imposed using the controlled mass flow meter, one can understand how the O/F was decreasing despite the G_{ox} was grown. The corresponding increasing of the regression rate values for both the fuel formulations, can be considered strictly linked with the previous consideration.
As it can be seen, the higher is the LAH content the higher is the calculated adiabatic flame temperature. The values of specific impulse, obtained imposing 12 bar as combustion pressure and a P_i/P_{ext} ratio of 12, were observed to be quite stable despite ($242.6 < I_{sp} < 242.9$) the adding of LAH.
Table 5 points out that regression rates measured using a fiber optic sensor (local and quasi-continous method) are higher than those measured using the mass variation technique (averaged in space and time) for formulations without LAH filler. The agreement of the two methods is, on the contrary, quite satisfactory for formulations added with LAH. Results show the remarkable decrease of the regression rate when the formulation includes a filler content.

Table 5. Results of the ballistic characterization.

Material	r_f (FO) [mm/s]	r_f (Δm) [mm/s]	P [bar]	G_{ox} [Kg/m^{2}s]	O/F	Φ	T_f [K]	I_{sp} [s]
S05G	2.70	1.54	7.1	72.4	1.96	1.74		
	2.66	1.72	8.6	90.5	2.32	1.47	3468	242.6
	2.31	1.98	10.4	108.6	2.34	1.46		
S05G-L5	1.11	1.20	7.7	72.4	2.54	1.41	3475	242.5
	1.34	1.56	9.9	90.5	2.44	1.47		
S05G-L10	0.95	1.11	9.7	72.4	2.70	1.39	3489	242.7
	0.95	1.34	12.6	90.5	2.99	1.25		
S10G	2.28	1.38	7.6	72.4	2.21	1.54	3473	242.8
	2.32	1.44	10.1	90.5	2.74	1.24		
S10G-L5	0.94	1.13	8.2	72.4	3.29	1.09	3479	242.8
	0.99	1.04	9.2	90.5	3.70	0.97		
S10G-L10	0.96	0.84	9.3	72.4	3.59	1.04	3493	242.9
	0.96	1.20	13.3	90.5	3.38	1.11		

Figure 12 shows a definite difference between the fuel surface, after a firing test, of formulations containing or not the filler. The surface of a S10G-L5 sample exhibits an irregular appearance due to the presence of carbonaceous formations. Cavities, below the fuel surface, can be observed; they are caused by LAH dehydrogenation and are not observable in all the formulations without LAH. The characteristic size of these cavities spans from 100 to approximately 500 μm, with a decrease in size moving from the surface towards the depth of the fuel.

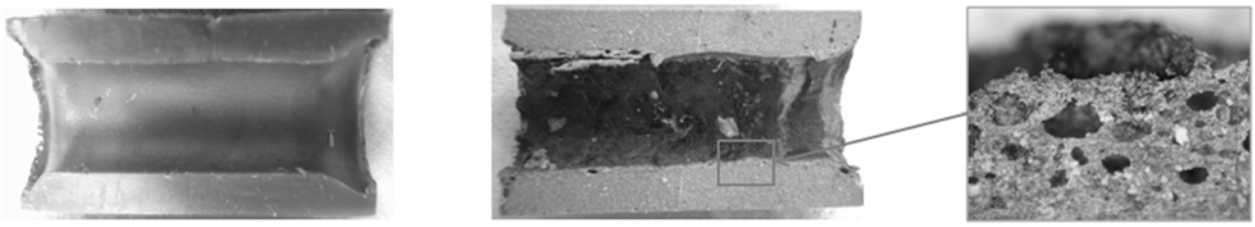

Figure 12. S10G-based mixtures cut along the plane of symmetry. S10G (left), S10G-L5 (center) and a magnification of the combustion surface of S10G-L5 (right).

The rough and irregular surface of a S05G-L5 sample, cut along the symmetry plane, is shown in Figure 13. The sample section, shown in the magnification of Figure 13b, exhibits a dark region, approximately 2 mm thick, immediately below the fuel surface. Figures 14 and 15 show the results of a DSC investigation of the material taken between 0 and 1 mm, 1 and 2 mm, 2 and 3 mm below the fuel surface. The position of the melting endothermic peaks is not affected by the depth. The degradation of LAH occurs between 150 and 190 °C; immediately below the fuel surface the amount of LAH is very low. It increases moving from the surface towards the virgin fuel, getting up the value of the fresh material moving beyond a distance of 2 mm. The ΔH_{dec} values, reported in Table 6, allow confirming this trend. A similar trend can be observed considering the decomposition occurring between 200 and 300 °C. Magnifications shown in Figures 14 and 15 point out that when the distance from the fuel surface increases, also ΔH_{dec} increases, up to the values obtained when the fresh material is tested.

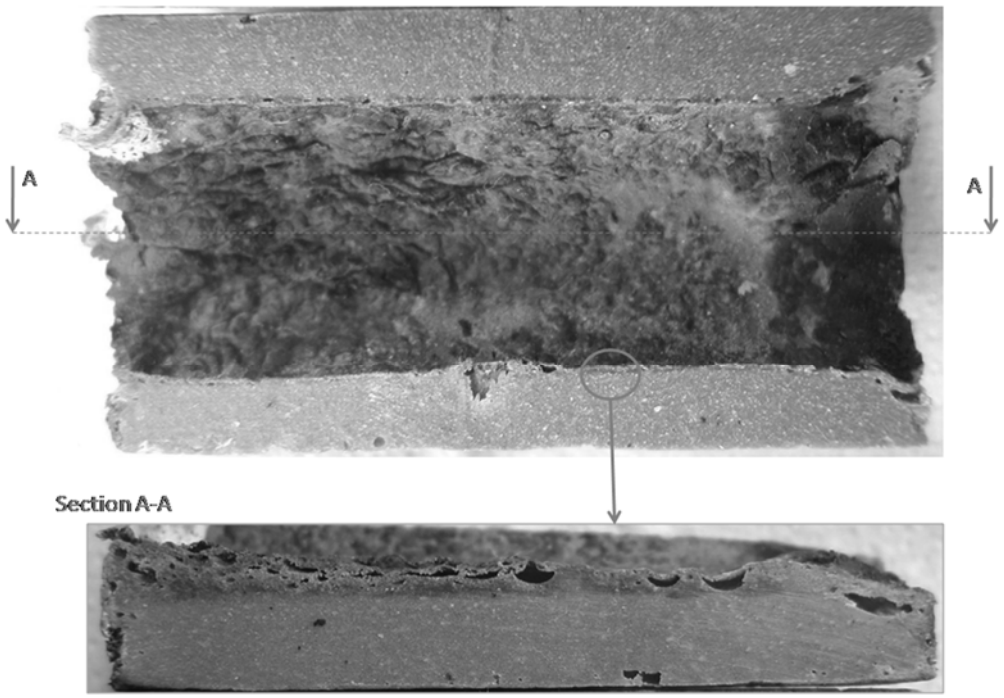

Figure 13. S05G-L5 cut along the plane of symmetry. An overview of the combustion surface (at the top) and a magnification of the material (at the bottom) just below the combustion surface. A change in colour between the partially pyrolyzed material and the fresh mixture can be observed.

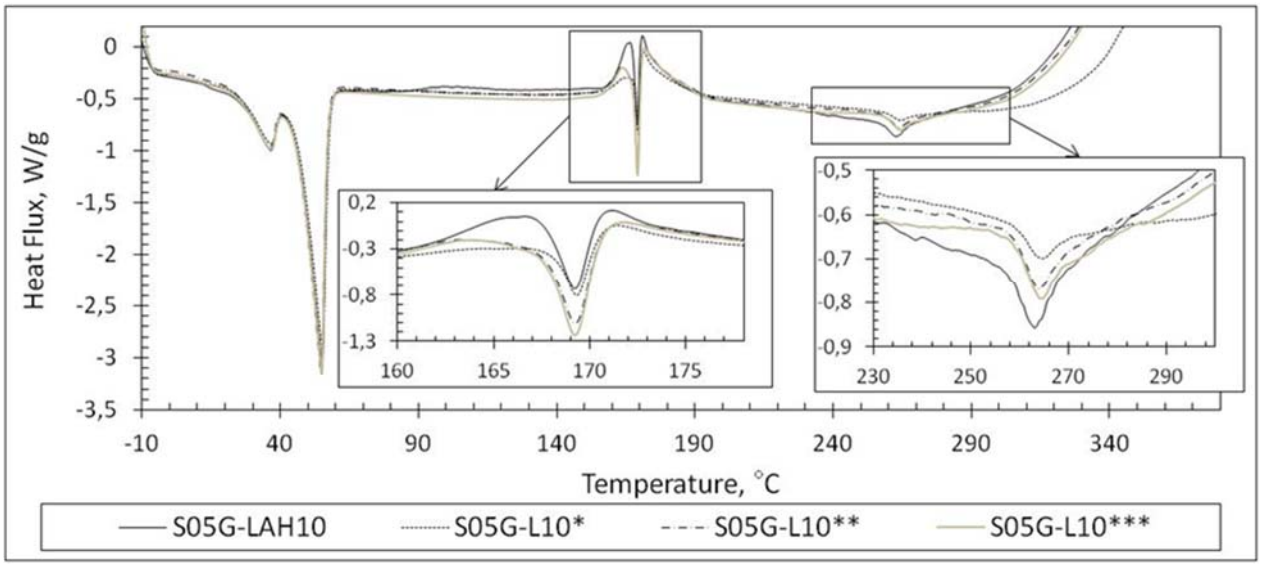

Figure 14. Comparison of DSC trend of S05G-L10 mixture. The black line represents the fresh material, while the other traces are linked with a sample burned at 4.55 g/s of pure oxygen. Each sample was taken at different depths below the combustion surface.

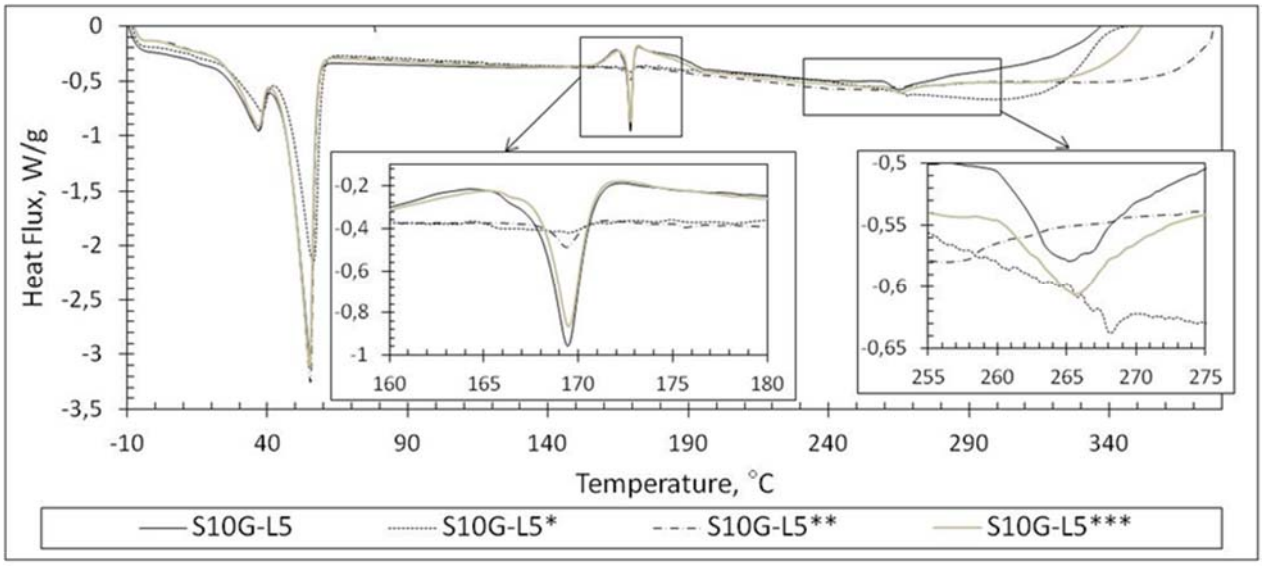

Figure 15. Comparison of DSC trend of S10G-L5 mixture. The black line represents the fresh material, while the other traces are linked with a sample burned at 4.55 g/s of pure oxygen. Each sample was taken at different depths below the combustion surface.

Table 6: Parameters obtained from DSC measurements for paraffinic waxes.
('T' temperature, 'ΔH' specific enthalpy, 'm' melting, 'dec' decomposition, 'f' fresh
'*' up to 1mm below the combustion surface (c.s.), '**' between 1 and 2 mm below the c.s., '***' 3 mm below the c.s.).

Material	Mass [mg]	$T_{m,p}$ 1 [°C]	$T_{m,p}$ 2 [°C]	ΔH_m [J/g]	T_{dec} 1 [°C]	T_{dec} 2 [°C]	T_{dec} 2 [°C]	ΔH_{dec} [J/g]	T_{dec} 1 [°C]	ΔH_m [J/g]
S05G*	2.99	36.6	55.0	204.3	-	-	-	-	265.3	137.5
S05G**	3.00	36.8	55.4	192.7	-	-	-	-	270.1	143.9

S05G[f]	2.90	36.7	55.3	198.3	-	-	-	-	273.2	154.9
S05G-L5[*]	2.92	36.6	55.0	192.3	-	172.0	-	-	264.4	47.9
S05G-L5[**]	2.98	36.8	55.2	199.1	-	-	-	-	262.7	47.6
S05G-L5[***]	2.92	36.6	55.0	197.0	164.9	169.2	171.3	25.1	264.1	37.5
S05G-L5[f]	2.90	36.4	55.1	193.2	164.4	169.2	171.6	24.83	264.7	24.9
S05G-L10[*]	3.00	36.7	55.1	174.0	164.4	169.3	171.5	29.7	263.7	29.1
S05G-L10[**]	2.99	36.3	54.9	188.6	163.2	169.2	171.7	38.2	263.9	56.5
S05G-L10[***]	3.02	36.6	55.0	183.9	163.9	169.2	171.8	39.9	264.5	59.4
S05G-L10[f]	2.91	36.7	55.2	181.1	166.6	169.2	171.1	46.5	263.1	84.6
S10G[*]	2.95	37.2	55.5	178.3	-	-	-	-	261.6	35.7
S10G[**]	2.98	36.7	55.0	192.2	-	-	-	-	265.5	92.6
S10G[f]	2.96	37.4	55.2	188.6	-	-	-	-	278.2	92.1
S10G-L5[*]	2.98	38.3	56.4	152.4	-	169.6	-	0.9	299.4	-
S10G-L5[**]	2.92	36.7	55.1	200.9	-	169.4	-	-	~250	30.7
S10G-L5[***]	2.93	36.9	55.2	191.5	165.3	169.5	172.3	19.4	265.7	28.7
S10G-L5[f]	2.81	37.0	55.2	179.2	164.4	169.4	172.3	18.5	265.1	45.3
S10G-L10[*]	2.94	37.6	55.0	128.5	-	169.2	-	13.6	263.2	24.6
S10G-L10[**]	3.01	37.2	55.4	176.3	165.4	169.5	171.9	43.1	263.7	47.3
S10G-L10[***]	3.00	36.8	55.0	169.7	164.8	169.4	171.9	40.1	264.0	76.9
S10G-L10[f]	2.86	36.9	55.2	171.3	164.2	169.5	172.3	48.3	264.1	94.7

The following step was the study of the mechanical properties of the material below the fuel surface in order to understand the causes of a lower regression rate of the formulations added with LAH, compared to those of non-added formulations. Figure 16 shows the behavior of the elastic modulus G' for the decomposed material taken from the surface of S05G-L5 and S05G-L10 fired samples, compared to the homologous fresh material. DSC traces are also compared. All the materials studied and reported on the plot show the same rheological behavior at low temperature values: two clearly visible drop in G' values (A and B) due to the corresponding paraffin wax transitions: solid-solid and solid-liquid transition. All the fresh materials, filled and unfilled with LAH, show a limit temperature of 52 °C at which the sensibility of the rotational rheometer is too low. As it can be seen considering the burned fuels (S05G-L5 and S05G-L10), a clear difference with the previous thermo-rheological behavior can be detected. All the fuel formulations rheologically tested after a firing test show an increase of the limit temperature detectable by using the rotational rheometer. S05G-L5 sample, rheologically studied after a firing test (empty triangles), shows a small increase of the melting temperature (C). After reaching the limit temperature of 71 °C, the material undergoes the complete melting. The material S05G-L10 decomposed by combustion (empty circles) becomes thermosetting, allowing rheological test continuation up to 220 °C (D); the fresh material (empty squares) exhibits a limit temperature of 52 °C (B). A clear difference between S05G-L5 and S05G-L10 (samples collected from the combustion surface after a firing test in the same experimental conditions) can be easily detected considering the respective limit temperature values (71 °C Vs. 220 °C). This large difference is linked with a strong change in the nature of the material: from thermoplastic to thermosetting and it could be ascribed with the content of LAH.

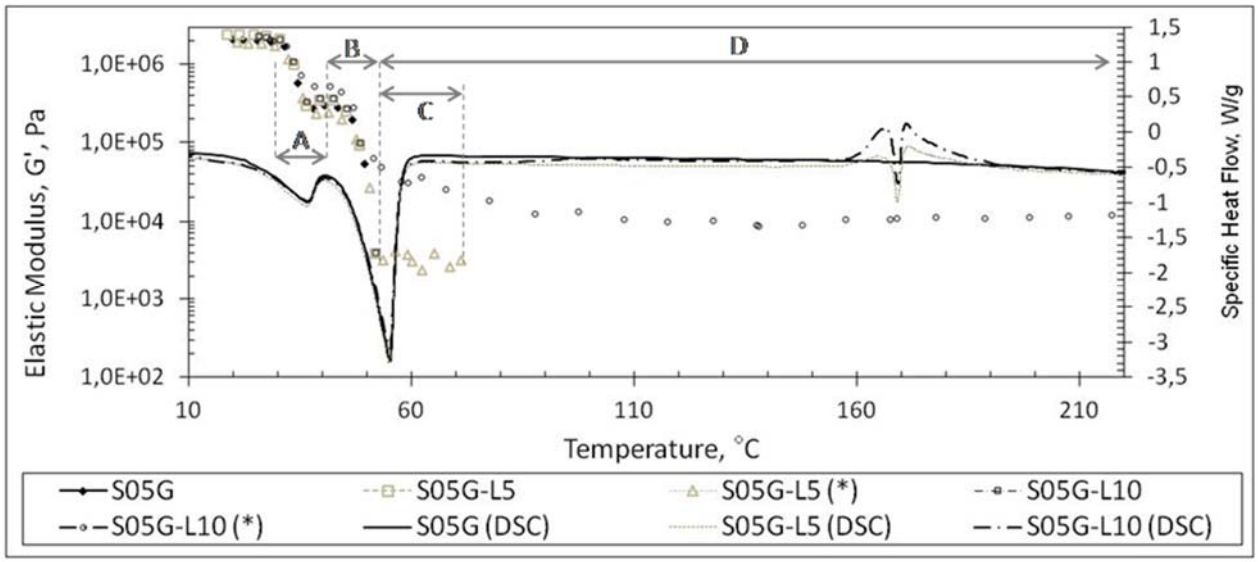

Figure 16. Comparison of G' and DSC trend of S05G-L5 and S05G-L10 mixtures tested fresh and after (*) a firing test. The material collected 2 mm below the combustion surface extinguished after a firing test studied with the rheometer.

A possible explanation of the poor results in terms of regression rates obtained with the LAH addition can be linked to the curing of the Paraffin/SEBS mixture. Viscosity increases, entrainment effects decrease and the material, initially thermoplastic, becomes thermosetting. The heating of the fuel at the surface, involves the hydride decomposition due to high temperatures. The presence of Lithium and Hydrogen activate "carbolithiation" reactions, which are responsible for thermoplastic polymers curing. The fuel at the surface does not melt and does not form a liquid film; diffusion flame mechanisms, typical of classical fuels, occur. Mechanisms of anionic polymerization, performed using alkyl-lithium initiators (R^-Li^+) are described by Dufton (2001).
One of the most important applications of Lithium-alkyl compounds is as polymerization initiator for diene-polymers. Metallic Sodium was used to initiate the polymerization reaction of butadiene obtaining BUNA (Butadiene-Natrium). A remarkable improvement of this method, as suggested by Pittalis (2007), was carried out by using n-BuLi (Lithium-alkyl) as chemical initiator. Butyllithium (n-BuLi) and other organolithium compounds are widely used in the production of elastomers (thermosetting: HTPB, polyisoprene; thermoplastic: styrene-butadiene SBS, SEBS, SIS); the reaction is named "`carbolithiation"':

4. CONCLUSIONS

In this work paraffin-based fuels, added with two different mass fractions (5 and 10%) of Lithium Aluminum hydride, were investigated. For the strengthening of paraffin waxes a styrene-based thermoplastic elastomer (Polystyrene-*block*-poly(ethylene-*ran*-butylene)-*block*-polystyrene grafted with maleic anhydride, SEBS-MA) was considered. An investigation of the thermal, rheological, mechanical and ballistic behavior of these blends was performed in order to reach a good trade-off between mechanical and ballistic properties.
The overlapping of DSC thermographs (the contribution of SEBS-MA cannot be detected by DSC, due to its amorphous nature) and elastic modulus traces, confirm the presence of critical temperature values (T_{mp-1} and T_{mp-2} corresponding to the solid-solid transition and solid-liquid transition of the paraffin wax respectively) which explain the rheological behavior of paraffin wax blended with SEBS-MA. This polymer, mixed with different mass fractions, improves

paraffin mechanical properties while the presence of LAH improves the fuel energetic content. It was observed a worsening of the ballistic properties of the LAH-based formulations, with a clear decrease of the regression rate values with respect to that typical of unfilled formulations. To explain this behavior an extensive study of thermal and rheological properties of samples taken from LAH-based fuels burned in a lab-scale hybrid rocket test bench has been performed. In particular it has been demonstrated that, in particular conditions, a SEBS and paraffin wax-based fuel can turn, from a thermoplastic to a thermosetting behaviour. As a consequence of that, the viscosity of the liquid film at the fuel surface increases decreasing, at the same time, the entrainment effect and so the regression rate.
A possible explanation of this strange behaviour could be ascribed to the well-known catalytic properties of Lithium-based metal-organic compounds which are extensively used to obtain a number of thermoplastic styrene-based elastomers. It should be possible that, at high temperature values typical of a firing test, the thermal decomposition of LAH leads to the formation of highly reactive chemical compounds, able to react with all the molecular fragments originated by the pyrolysis process of SEBS-MA and wax. These kind of chemical reactions, which normally do not occur at low temperature values typical of rheological tests, could explain the reason why the post-firing test materials containing LAH, can be rheologically tested up to temperature values much higher than that typical of unfilled wax-based fuels.

Further studies are needed to explore the interaction between LAH and a paraffin-based fuel thoughened with SEBS-MA, both from a chemical, ballistic and rheological point of view.

ACKNOWLEDGEMENTS

The authors would like to thank Jelly Wax Srl (http://www.jellywax.it) for the support, sharing experience and paraffin procurement.

REFERENCES

Alcazar-Vara L.A., and Buenrostro-Gonzalez E., (2013). Liquid-Solid Phase Equilibria of Paraffinic Systems by DSC Measurements, *InTech*, Chap. 11, ISBN 978-953-51-0947-1.

Altman, D., (2003). Highlights in Hybrid Rocket History, in L.T. DeLuca Ed., *8-IWCP-Rocket Propulsion: Present and Future*, grafiche g.s.s, Bergamo, Italy, September 2003.

Asthana S., and Kennedy J.P., (2002). Novel Polyisobutylene Stars. XXIII. Thermal, Mechanical and Processing Characteristics of Poly(phenylene ether)/Polydivinylbenzene(polyisobutylene-b-polystyrene)$_{37}$ Blends, *J. Appl. Polym. Sci.*, Vol. 86, pp. 2866 – 2872.

Benterou, J., Udd, E., (2007). Measurements Using Fiber-optic Bragg Grating Sensors. EuroPyro, 34th International Pyrotechnics Seminar, Beaune, France.

Block. J., and Gray. A.P., (1964). The Thermal Decomposition of Lithium Aluminum Hydride, *Inorganic Chemistry*. Vol. 4, No. 3, pp. 304–305.

Boiocchi. M., Merotto. L., Galfetti. L., (2012). Paraffin-based Fuel Filled with Lithiumbased Additives Characterization, 63rd International Astronautical Congress, Naples, Italy, 1–5 Oct 2012, IAC-12-C4.2.27

Boiocchi, M., Milova, P., Galfetti, L., Di Landro, L., and Golovko, A. K., A wide characterization of paraffin-based fuels mixed with styrene-based thermoplastic polymers for hybrid propulsion, Prog. Propul. Phys. B, vol. 8, pp. 241–262, 2016.

Chazhengina, S.Y., Kotelnikova, E.N., Filippova, I.V., and Filatov, S.K., (2003). Phase Transition of n-Alkanes as Rotator Crystals, *J. Mol. Struct*. Vol. 647, pp. 243.

Chiaverini, M.J., Serin, N., Johnson, D., Lu, Y.C., Kuo, K.K. and Risha, G.A., (2000). Regression Rate Behavior of Hybrid Rocket Solid Fuels, *Journal of Propulsion and Power*, Vol. 16, No. 1, pp. 125–132.

Chow W.S., Leu Y.Y., and Mohd Ishak Z.A., (2012). Effects of SEBS-g-MAH on the Properties of Injection Moulded Poly(lactic acid)/nano-Calcium Carbonate Composites, *eXPRESS Polymer Letters*, Vol. 6, No. 6, pp. 503 – 510.

Davydenko, N.A., Gollender, R.G., Gubertov, A.M., Mironov, V.V., and Volkov, N.N., (2007). Hybrid Rocket Engines: The Benefits and Prospects, *Aerospace Science and Technology* 11, pp. 55–60.

Dezhen W., Wang X., and Jin R., (2004). Toughening of Poly(2,6-dimethyl-1,4-phenylene oxide)/nylon 6 Alloys with Functionalized Elastomers Via Reactive Compatibilization: Morphology, Mechanical Properties and Rheology, *Eur. Polym. J.*, Vol. 40, pp. 1223 – 1232.

Dufton, P.W., (2001). *Thermoplastic Elastomers*, iSmithers Rapra Publishing, pp. 8-10.

Galfetti, L., Merotto, L., Boiocchi, M., Maggi, F., and De Luca, L., Ballistic and rheological characterization of paraffin-based fuels for hybrid rocket propulsion, in Proc. of 47th AIAA/ASME/SAE/ASEE Joint Propulsion Conference and Exhibit, San Diego, CA, AIAA Paper 2011-5680, 2013.

Horiuchi S., Matchariyakul N., Yase K., and Kitano T., (1997). Compatibilizing Effect of Maleic Anhydride Functionalized SEBS Triblock Elastomer Through a Reaction Induced Phase Formation in the Blends of Polyamide6 and Polycarbonate: 2. Mechanical Properties, *Polymer*, Vol. 38, No. 1, pp. 59 – 78.

Huang J. J., Keskkula H., and Paul D.R., (2006). Elastomer Particle Morphology in Ternary Blends of Maleated and non-Maleated ethylene-based Elastomers with Polyamides: Role of Elastomer Phase Miscibility, *Polym*er, Vol. 47, pp. 639 – 651.

Humble, R.W., (2000). Fuel Performance Enhancements for Hybrid Rockets, *36th AIAA/ASME/SAE/ASEE Joint Propulsion Conference and Exhibit*, Huntsville, Alabama. AIAA Paper 2000-3437.

Karabeyoglu, M.A., Cantwell, B.J., and Altman, D., (2001). Development and Testing of Paraffin-Based Hybrid Rocket Fuels, *37th AIAA/ASME/SAE/ASEE Joint Propulsion Conference and Exhibit*, Salt Lake City, Utah. AIAA Paper 2001-4503.

Karabeyoglu, M.A., Zilliac, G., Cantwell, B.J., DeZilwa, S., and Castellucci, P., (2004). Scale-Up Tests of High Regression Rate Paraffin-Based Hybrid Rocket Fuels, *Journal of Propulsion and Power*, Vol. 20, No. 6, pp. 1037–1045.

Karabeyoglu, M.A. and Cantwell, B.J., (2002). Combustion of Liquefying Hybrid Propellants: Part 2, Stability of Liquid Films. *Journal of Propulsion and Power*, Vol. 18, No. 3, pp. 621–630.

Kim J.K., Paglicawan M.A., and Balasubramanian M., (2006). Viscoelastic and Gelation Studies of SEBS Thermoplastic Elastomer in Different Hydrocarbon Oils. *Macromolecular Research*, Vol. 14, No. 3, pp. 365-372.

Kleppinger R., van Es M., Mishenko N., Koch M.H.J., and Reynaers H., (1998). Physical Gelation in a Triblock Copolymer Solution: In Situ Study of Stress-Strain Behavior and Structural Development, *Macromolecules*, Vol. 31, pp. 5805.

Kleppinger R., Mishenko N., Reynaers H., and Koch M.H.J., (1999). Long-Range Order in Physical Networks of Gel-Forming Triblock Copolymer Solutions, *J. Polym. Sci.; Part B: Polym. Phys.*, Vol. 37, pp. 1833.

Laurer J.H., Mulling J., Khan S.A., Spontak R., and Bukovnik R., (1998). Thermoplastic Elastomer Gels. I. Effects of Composition and Processing on Morphology and Gel Behavior, *J. Polym. Sci.; Part B: Polym. Phys.*, Vol. 36, pp. 2379.

Laurer J.H., Mulling J., Khan S.A., Spontak R., and Bukovnik R., (1998).Thermoplastic Elastomer Gels. I. Effects of Composition and Temperature on Morphology and Gel Rheology, *J. Polym. Sci.; Part B: Polym. Phys.*, Vol. 36, pp. 2513.

Laurer J.H., Bukovnik R., andSpontak R.J., (1996). Morphological Characteristics of SEBS Thermoplastic Elastomer Gels, *Macromolecules*, Vol. 29, pp. 5760.

Litmanovich A.D., Platé N.A., and Kudryavtsev Y.V., (2002). Reactions in Polymer Blends: Interchain Effects and Theoretical Problems, *Prog. Polym. Sci.*, Vol. 27, pp. 915 – 970.

Maruyama S., Ishiguro, T., Shinohara, K. and Nakagawa, I., (2011). Study on Mechanical Characteristics of Paraffin-Based Fuel. *47th AIAA/ASME/SAE/ASEE Joint Propulsion Conference & Exhibit*, 31 July-3 August, San Diego, CA.

McLain W., and Honea. F., (1969). Pyrolysis and Combustion of Lithium Aluminum Hydride. AFOSR 69-2052TR.

Mingjie Zheng, and Weimin Du, (2006). Phase Behavior, Conformations, Thermodynamic Properties, and Molecular Motion of Multicomponent Paraffin Waxes: a Raman Spectroscopy Study, *Vibrational Spectroscopy*, Vol. 40, pp. 219 – 224.

Oiknine, C., (2006). New Perspectives for Hybrid Propulsion, 42nd AIAA Aerospace Sciences Meeting and Exhibit, Sacramento, California. AIAA 2006-4674.

Osmon, R.V., (1966). An Experimental Investigation of a Lithium Aluminum Hydride-Hydrogen Peroxide Hybrid Rocket. *Aerospace Chemical Engineering*, Vol. 62. No. 61.

Pittalis, M., (2007). *I* Metalli Alcalini in Sintesi Organica: Attivazione e Selettività del Sodio Metallico in Reazioni di Metallazione Riduttiva, Ph.D. Thesis, Università Degli Studi di Sassari.

Pracella M., Haque M., and Alvarez V., (2010). Functionalization, Compatibilization and Properties of Polyolefin Composites with Natural Fibers, *Polymers*, Vol. 2, pp. 554 – 574.

Prasman E., (1997). Morphology and Mechanical Behavior of Oriented Blends of Styrene-Isoprene-Styrene Triblock Copolymer and Mineral Oil, Master thesis, Massachussets Institute of Technology.

Reynders K., Mishenko N., and Mortensen K., (1995). Stretching-induced Correlations in Triblock Copolymer Gels as Observed by Small-Angle Scattering, *Macromolecules*, Vol. 28, pp. 8699.

Royon L., and Guiffant G., (2001). Heat Transfer in Paraffin oil/water Emulsion Involving SupercoolingPhenomenon, *Energy Conversion and Management*, Vol. 42, pp. 2155 – 2161.

Seno J., and Selvin Thomas P., (2006). Thermal and Crystallisation Behaviours of Blends of Polyamide 12 with Styrene–Ethylene/Butylene Styrene Rubbers, *Polymer,* Vol. 47, pp. 6328-6336.

Shark S., Pourpoint T.L., Son S., and Heister S.D., (2013). Performance of Dicyclopentadiene/H2O2-based Hybrid Rocket Motors with Metal Hydride Additives, Journal of Propulsion and Power, Vol. 29, Issue 5, pp. 1122-1129.

Udd, E., Benterou, J., (2010). Review of High-Speed Fiber Optic Grating Sensors Systems. SPIE Defense, Security and Sensing, 7677-Fiber Optic sensors and Applications VII, Orlando, United States.

Wang J., Calhoun M.D., and Severtson S.J., (2008). Dynamic Rheological Study of Paraffin Wax and its Organoclay Nanocomposites, *J. Appl. Polym. Sci.*, Vol. 108, pp. 2564 – 2570.

Wilkinson A.N., Laugel M.L., Clemens V.M., Harding V.M., and Marin M., (1999). Phase Structure in Polypropylene/PA6/SEBS Blends, *Polymer*, Vol. 40, pp. 4971 – 4975.

Wilkinson A.N., Clemens M.L., and Harding V.M., (2004). The Effect of SEBS-g-maleic Anhydride Reaction on the Morphology and Properties of Polypropylene/PA6/SEBS Ternary Blends, *Polymer*, Vol. 45, pp. 5239 – 5249.

Zhang Q., Song S., Feng J., and Wu P., (2012). A New Strategy to Prepare Polymer Composites with Versatile Shape Memory Properties, *Journal of Materials Chemistry*, Vol. 22, pp. 24776.

Zheng, M. and Du, W., Phase behavior, conformations, thermodynamic properties, and molecular motion of multicomponent paraffin waxes: A Raman spectroscopy study, *Vib. Spectrosc*., vol. 40, no. 2, pp. 219–224, 2006.